Analytica Chimica Acta 905 (2016) 58–65

Contents lists available at ScienceDirect

Analytica Chimica Acta

journal homepage: www.elsevier.com/locate/aca

Tunable nanogap devices for ultra-sensitive electrochemical impedance biosensing

Yong Lu [a], Zheng Guo [b], Jing-Jing Song [a], Qin-An Huang [a], Si-Wei Zhu [a], Xing-Jiu Huang [b], Yan Wei [a, *]

[a] Department of Chemistry, Wannan Medical College, Wuhu 241002, PR China
[b] Nanomaterials and Environmental Detection Laboratory, Institute of Intelligent Machines, Chinese Academy of Sciences, Hefei 230031, PR China

HIGHLIGHTS

- A tunable gold nanogap device was used as to *electrochemical impedance* biosensor.
- Linear range from 1 pM to 100 nM with LOD of 1 pM for streptavidin detection was obtained.
- The nanogap devices exhibit a satisfactory precision, stability, and reproducibility.
- The combination of *electrochemical impedance* technique and nanogap devices was achieved.

GRAPHICAL ABSTRACT

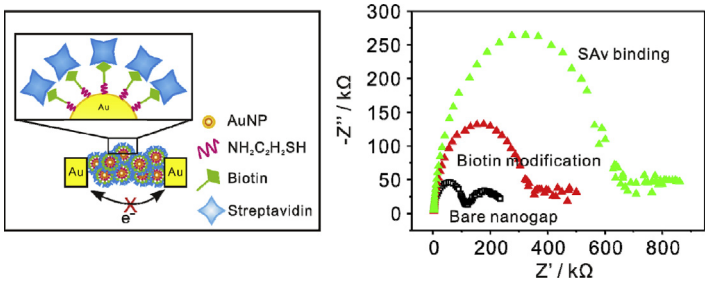

ARTICLE INFO

Article history:
Received 9 October 2014
Accepted 29 November 2015
Available online 17 December 2015

Keywords:
Tunable nanogap devices
Streptavidin
Electrochemical impedance
Ultra-sensitive
Electron-transfer resistance

ABSTRACT

A wealth of research has been available discussing nanogap devices for detecting very small quantities of biomolecules by observing their *electrical* behavior generally performed in dry conditions. We report that a gold nanogapped electrode with tunable gap length for ultra-sensitive detection of streptavidin based on *electrochemical impedance* technique. The gold nanogap is fabricated using simple monolayer film deposition and *in-situ* growth of gold nanoparticles in a traditional interdigitated array (IDA) microelectrode. The electrochemical impedance biosensor with a 25-nm nanogap is found to be ultra-sensitive to the specific binding of streptavidin to biotin. The binding of the streptavidin hinder the electron transfer between two electrodes, resulting in a large increase in electron-transfer resistance (R_{et}) for operating the impedance. A linear relation between the relative R_{et} and the logarithmic value of streptavidin concentration is observed in the concentration range from 1 pM (picomolar) to 100 nM (nanomolar). The lowest detectable concentration actually measured reaches 1 pM. We believe that such an electrochemical impedance nanogap biosensor provides a useful approach towards biomolecular detection that could be extended to a number of other systems.

1. Introduction

Nanogap devices for biosensing have emerged as a powerful technique for detecting very small quantities of biomolecules. Specific area of interest includes recent great developments in *electrical* nanogap (planar and vertical nanogap) for biosensing due to that the most charming feature of the devices is to directly transduce events of biomolecules specific binding into useful electrical signals such as resistance/impedance, capacitance/dielectric, or field-effect [1]. In

* Corresponding author.
E-mail address: yanwei_wnmc@hotmail.com (Y. Wei).

http://dx.doi.org/10.1016/j.aca.2015.11.036
0003-2670/

recent work by Gao and co-workers, a new method that allows nanogapped microelectrode for the ultrasensitive (that is, in a range from femtomolar (fM) to picomolar (pM), detection limit is in fM level) electrical detection of microRNAs (miRNAs) and nucleic acids as well as oligonucleotide has been reported [2–4]. The novel approach operates by depositing polyaniline (PAn) onto the hybridized miRNA strands [2], by introducing silver nanoparticles on the hybridized DNA [3], and using an aggregate of gold nanoparticles in a microgap as a conductive tag [4]. The same author used hybridization and subsequent metallization of the two termini of a target DNA with two different surface-bound capture probes to bridge the nanogap for the quantification of DNA based on electronic transduction [5]. Using similar concept, they created an electrical sensor array for polymerase chain reaction-free messenger RNA expression profiling [6]. In a similar vein, the researchers has also specifically designed an electronic sensor for label-free detection of single-nucleotide polymorphisms relying on building target DNA-templated silver nanowires (conductive paths) across a nanogap [7].

A number of research groups including ours have been investigating *electrical* detection of biomolecules based on nanogapped gold particle film in dry surface of the devices. Using ethanolic decanedithiol as a binder, the Nagaoka group have presented nanogapped gold nanoparticle array for DNA detection [8–13]. Similar work by Nie and Huang has used self-catalytic growth of unmodified gold nanoparticles as conductive bridges mediated gap-electrical signal transduction for DNA hybridization detection [14]. We have introduced CdSe quantum dot-labeled streptavidin in nanogap devices to boost electrical signals for biotin-streptavidin sensing events [15]. Also, HS-β-Cyclodextrin (β-CD) was introduced onto the gold nanogapped electrodes' surface for capturing polychlorinated biphenyls (PCBs) [16]. Through a self-assembling technique, we have designed a molecular-gap device for specific electrical determination of trace Hg^{2+} by a thin film of glutathione monolayer capped Au nanoparticles [17].

Nanogap electrochemical technique, one of new electrochemical methods [18], provides a great opportunity for detection of single-molecule by consideration of redox cycling of the electroactive species between the two closely neighboring electrodes, which allows each individual molecule could undergo multiple electron transfers [19,20]. On the other hand, as most biological species (e.g., antibodies and antigens) are electrochemically inert, electrochemical impedimetric biosensing has received much attention due to its high sensitivity and low cost [21,22]. Representative examples include detection of C-reactive protein (CRP) by specific binding of CRP antigen and CRP antibody on three-dimensionally ordered macroporous gold film [23], an Immunoglobin A (IgA) immunosensor based on colloidal carbon sphere array [24], and *Escherichia coli* O157:H7 (*E. coli*) immunobiosensors [25], as well as impedimetric biosensor for the assessment of the clotting activity of rennet [26]. In particular, *E. coli* cells could efficiently detected in a range from 4.36×10^5 to 4.36×10^8 cfu/mL with a detection limit of 10^6 cfu/mL based on the formation of antibody–antigen complexes at interdigitated array microelectrodes with 15-μm interdigit space [27]. Very recently, Willner investigated controlling interfacial electron transfer and electrocatalysis by pH- or ion-switchable DNA monolayer-modified electrodes [28].

Here, a tunable nanogap device for ultra-sensitive detection of biotin-streptavidin binding based on *electrochemical impedance* technique is reported. The device was fabricated on an interdigitated array microelectrode (IDAME), and the nanogap was created by depositing gold nanoparticles onto an IDAME substrate. The gap length is tunable by controlling the *in situ* growth time of gold nanoparticles. Gold nanoparticles were modified with self-assembled monolayers (SAM) of cysteamine, and then for biotin and biotin & streptavidin binding. The bindings of the SAM, biotin, and streptavidin in the nanogap were detected by measuring the change of the electron-transfer resistance, R_{et}. An electrical equivalent circuit was proposed for understanding stepwise changes in impedance components of nanogap device.

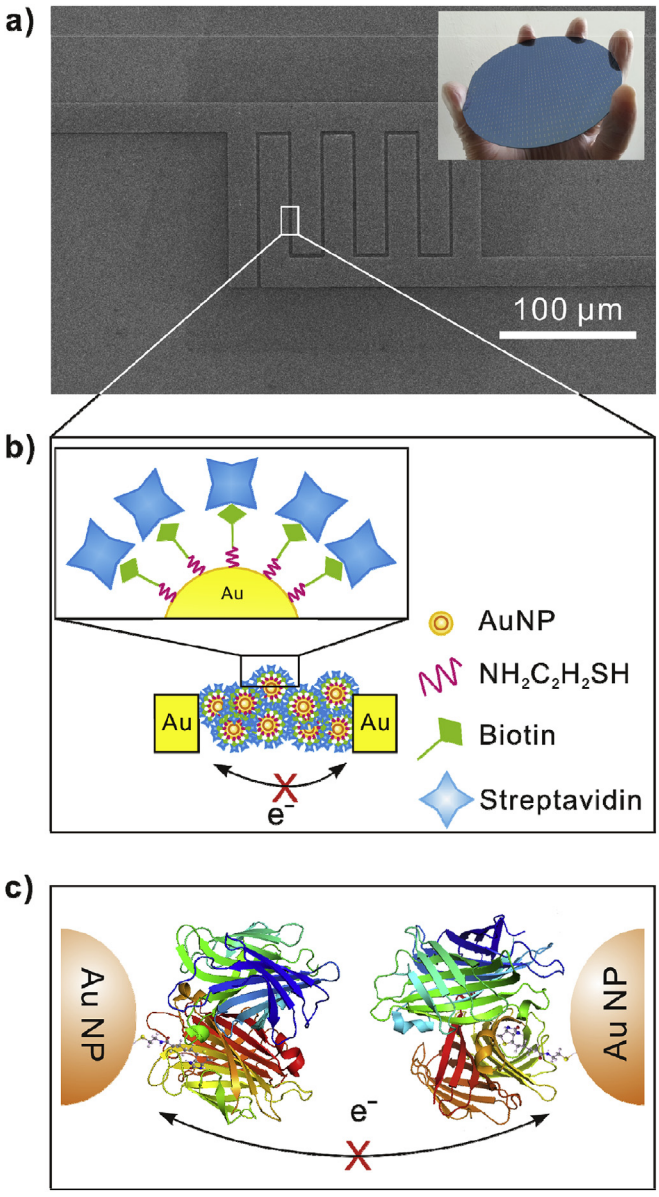

Fig. 1. a) SEM image of gold nanogapped electrodes referring to the narrow space between neighboring gold nanoparticles which is fabricated by a monolayer of gold nanoparticles film between two adjacent microelectrodes in the IDA microelectrode. Inset is a digital camera image of a 4-inch silicon wafer in which IDA microelectrodes were fabricated. b) Sensing mechanism of gold nanogapped devices. After exposure to the solution sample, some particles in the nanogap can capture target molecules, and the resistance of the film increases. The greater the amount of analyte, the more target molecules are captured on the surface of the Au NPs, and the higher the resistance. c) Functionalization of gold nanoparticles with a self-assembled monolayer of cysteamine followed by the attachment of biotion. The surface bound biotin serves as selective binding sites for streptavidin.

2. Experimental section

2.1. Chemical reagents

All the reagents used in this experiment were of analytical grade, and used as received without further purification. Potassium

ferricyanide ($K_3[Fe(CN)_6]$), potassium ferrocyanide ($K_4[Fe(CN)_6]\cdot 3H_2O$), KH_2PO_4, $Na_2HPO_4\cdot 2H_2O$, NaCl, KCl, Tween20, Chloroauric acid ($HAuCl_4$), trisodium citrate, hydroxylammine hydrochloride ($NH_2OH\cdot HCl$), borate (H_3BO_3), ethanol, and acetone were received from Sinopharm Chemical Reagent Co., Ltd., China. Phosphate-buffered saline solution (PBS; 0.1 M, pH 7.4) were prepared by dissolving 13.43 g of $Na_2HPO_4\cdot 12H_2O$ and 6.8 g of KH_2PO_4 in 500 ml of ultrapure fresh water. PBST solution was prepared using PBS solution and 0.05% (v/v) Tween20 and 50 mM borate buffer (pH 8.4) was prepared by dissolving 0.31 g H_3BO_3 in 100 mL of ultrapure fresh water. 3-Aminopropyl-trimethoxysilane (APTMS) and cysteamine hydrochloride were purchased from Aladdin. Biomoleculars sulfo–NHS–LC-biotin and streptavidin were obtained from Pierce. All of the solutions that used were prepared with ultrapure fresh water from a Millipore water purification system (Milli-Q, specific resistivity >18.25 MΩ cm, S.A., Molsheim, France).

2.2. Synthesis of colloidal gold nanoparticals

Gold nanoparticles (Au NPs) with an average diameter of about 16 nm were synthesized using the citrate reduction method introduced by Turkevitch et al. [29] and further developed by Frens [30]. All glass containers were cleaned in a bath of freshly prepared HCl/HNO_3 (3:1, v/v), rinsed thoroughly in ultrapure fresh water, and dried in an oven prepare for further use. 100 mL of 0.01% chlorauric acid ($HAuCl_4$) aqueous solution was brought to a rolling boil with stirring. Then 4 mL 1% trisodium citrate was added to the solution and mixed together. A very faint greyish-pink or greyish-blue tone would be observed in about 1 min, then gradually to black color over a period of about 5 min. After that, the mixture was boiled for 30 min, and then the solution was allowed to cool down to room temperature with continued rapid stirring. The Au NPs colloidal solution (light wine-red color) was stored in a refrigerator (4 °C) for further application.

2.3. Fabrication of nanogapped electrode

Prior to the fabrication, the interdigitated array microelectrode (IDA microelectrode) was cleaned in acetone bath for 2 h and then immersion in piranha solution (H_2SO_4: H_2O_2 = 7: 3, v/v) for 10 min in order to get rid of inorganic and organic contaminant on the substrate surface, followed by rinsing thoroughly with ultrapure fresh water and dried under nitrogen flow. Subsequently, 1 mM APTMS of absolute ethanol solution were utilized to treat the IDA microelectrode substrate for 2 h at room temperature. Then, the substrate was rinsed with absolute ethanol solution and ultrapure fresh water, dried under nitrogen flow, and the IDA microelectrode was placed in a 120 °C oven for 30 min to get a more sufficient and complete Si–O bond formation. Finally, the IDA microelectrode was immersed in the concentrated Au NPs colloidal solution which was obtained from using the prepared Au NPs colloidal solution centrifuged and washed twice with ultrapure fresh water for 8 h at room temperature.

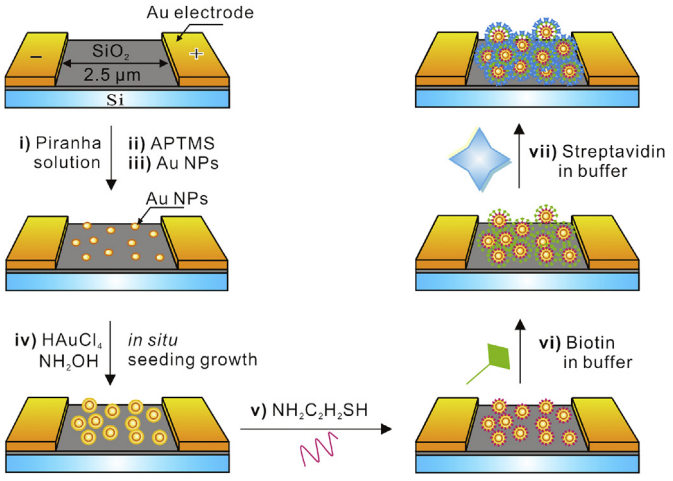

Fig. 2. Schematic diagram of a gold nanogapped electrode modified with biotin for streptavidin detection.

2.4. In situ seeding growth of gold nanoparticles

In order to get the appropriate nanogapped electrode device, the interval between neighboring Au NPs must be narrowed. The solution for Au NPs *in situ* seeding growth which was prepared by mixing together 0.01% $HAuCl_4$ and 0.4 mM $NH_2OH\cdot HCl$ freshly was applied. The IDA microelectrode was placed in the solution with continuously agitating to swirl the solution over the electrode surface. The size of the gap formed between neighboring Au NPs entirely depends on the reaction time, thus the reaction was allowed to continue at room temperature for 0, 0.5, 1, 1.5, 2, and 3 min, respectively, to obtain a set of nanogaps with different sizes. Finally, the surface was immediately washed with ultrapure fresh water and dried under nitrogen flow.

2.5. Biomoleculars self-assembly for detection of streptavidin

The cleaned nanogap device was placed into 3 mM ethanol solution of cysteamine hydrochloride at room temperature, followed by exhaustively washing using ethanol and ultrapure fresh water 4 h later, after which it was blow dried under nitrogen flow.

The nanogap electrode with cysteamine monolayer was then dipped into a fresh sulfo–NHS–LC-biotin PBS buffer (pH 7.4) solution for 10 h at room temperature followed by ultrapure fresh water and PBST solution washing to remove nonspecifically adsorbed biotin. After that, the fresh biotinylation nanogap device was immersed into the different concentrations of streptavidin borate buffer solution at room temperature for one day. The final device was rinsed extensively with PBS (pH 7.4) containing 0.05% Tween and ultrapure fresh water and blow drying in ultrapure nitrogen stream.

2.6. Electrochemical measurement

Electrochemical experiments were recorded using an AutoLab computer-controlled potentiostat (Eco Chemie, Utrecht, Netherlands) associated with the GPES software. One of the two pair interdigitated microelectrode array was used as reference/counter electrode; another was used as working electrode. The nanogapped electrode was submerged in 8 mL of 0.01 M PBS solution (pH 7.4) containing a pair of 10 mM redox couple $[Fe(CN)_6]^{3-/4-}$ (1:1) at room temperature. Cyclic voltammetry (CV) experiments were carried out with potential scanned from −0.4 V to 0.4 V at a scan rate of 100 mV/s. Electrochemical impedance spectroscopy (EIS) measurements were recorded from 0.1 Hz to 100 kHz with a 5 mV amplitude, sine wave was applied to the electrode at the half-peak potential (0 V) of the redox couple. Nyquist (imaginary impedance vs real impedance) and Bode (impedance and phase vs frequency) diagrams were recorded during the experiments. The EIS data were analyzed and simulated with commercial software ZSimpWin 3.2 version, fifty points of data from each measured spectrum were automatically selected by the software for input into equivalent circuits to generate a fitting spectrum.

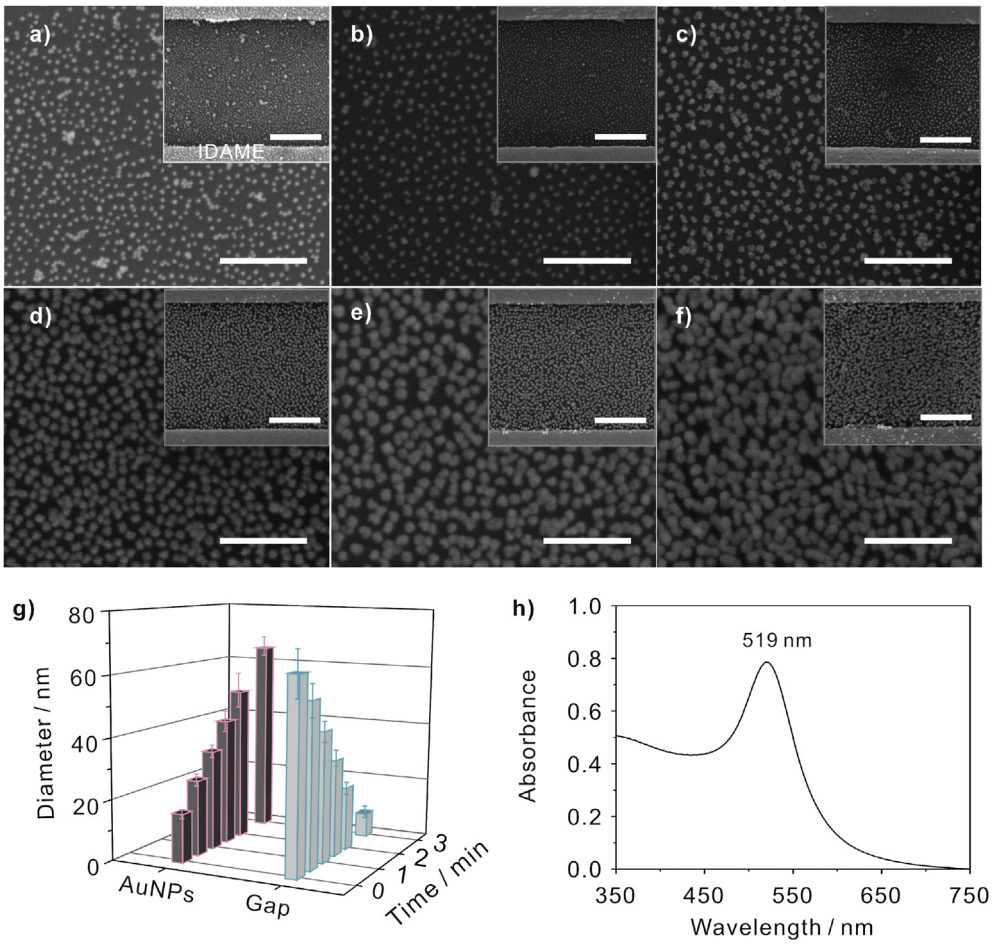

Fig. 3. a–f) SEM images of a monolayer gold nanoparticles which is uniform distribution in the 2.5-μm gap between two adjacent IDA microelectrodes after *in situ* seeding growth of 0, 0.5, 1, 1.5, 2, 3 min. Error bar: 500 nm. The insets in panels *a–f* are SEM images showing the corresponding 2.5-μm gap at low magnification. Error bar: 1 μm g) Relationship of the gold nanoparticles size and the length of the nanogap between neighboring gold nanoparticles with the *in situ* seeding growth time. e) UV spectrum of the synthesized Au NPs.

3. Results and discussion

Fig. 1 shows the concept of ultra-sensitive electrochemical impedance biosensor based on tunable nanogap devices. Fig. 1a is the SEM image of gold nanogapped electrodes fabricated on a silicon chip. The IDA microelectrode was manufactured by preparing gold patterns on silicon wafer (doped with boron, resistivity ~ 1–30 Ω cm) with 100 nm thick oxide layer on it to prevent leak current possibly occurringthrough the substrate according to conventional photolithographic method [2]. The IDA microelectrode consists of a pair of parallel microstrip electrodes that alternately connected and joggled with each other, thus it has some gaps and a group of interdigitating electrode fingers. The dimension of the microband length, width, and the interval between adjacent electrode fingers was 177.5 μm, 125 μm and 2.5 μm, respectively. The 2.5-μm space between two adjacent microelectrode fingers was consequently filled with gold nanoparticles. The gap size between neighboring gold nanoparticles could be well controlled by growth time. The biotin modified Au NPs assembled between two interdigitated electrodes are the biosensing particles. When put into a sample solution that contains streptavidin, some of biotin modified gold particles bind with the streptavidin in solution. Such films have high resistance. Fig. 1b shows the detection principle of the biosensor based on the specific binding between biotin and streptavidin. In a typical electrochemical impedance biosensor, two factors contribute to the conductivity change of nanogap device during the measurements: (1) the relative distances between neighboring gold nanoparticles, *d*; and (2) the relative dielectric constant after filling in the nanogap, ε_i. As depicted in Fig. 1b, the biotin molecules were modified on the surface of Au NPs as traps, when biomolecules are introduced into the nanogap, the specific binding between biotin and streptavidin could create a barrier for the electrochemical process, thereby hindering the access of the redox probe ($Fe(CN)_6^{3-/4-}$) to the electrode surface, resulting in an increase in the electron-transfer resistance. Thus, by monitoring the capacitance change, it is possible to detect the specific binding of streptavidin to biotin

Fig. 2 shows the constitution of nanogapped microelectrode and the detection mechanism of streptavidin based on the specific inhibition of electrons transfer by biomolecules. Firstly, the IDA microelectrode was cleaned with piranha solution before using. The cleaned electrode with 2.5-μm microgap was then put into3-aminopropyl-trimethoxysilane (APTMS) ethanol solution to make silanization treatment. The concentrated gold colloid solution was used to deposit a monolayer of Au NPs film on the surface of 2.5-μm microgap. Finally, the suitable nanogapped electrode was obtained by apply *in situ* seeding growth method to control the diameter of Au NPs and the gap size. A mercapto group on cysteamine connected to the gold nanoparticles in an alcoholic solution of cysteamine hydrochloride, an amino group on the other side of the cysteamine formed an amide bond with Sulfo–NHS–LC-biotin (sulfosuccinimidyl-6-[biotin-amido] hexanoate) in PBS buffer. The

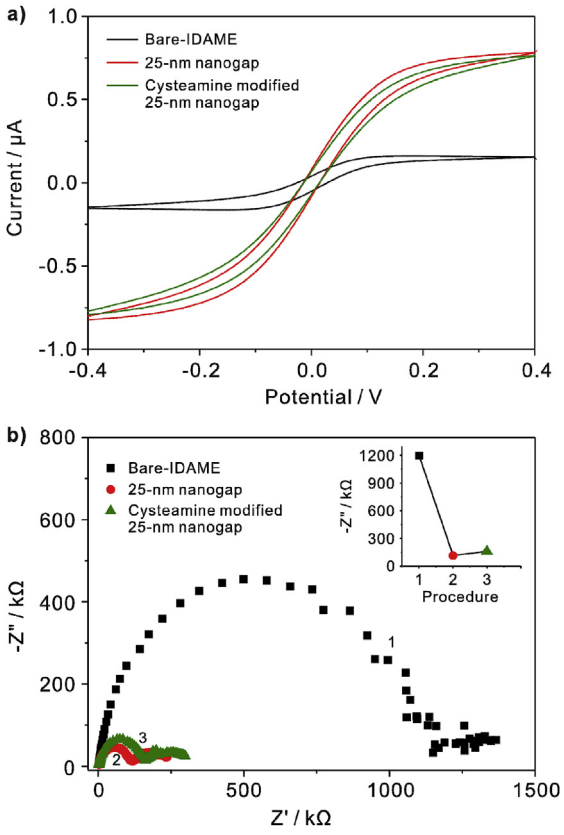

Fig. 4. a) Cyclic voltammograms and b) Nyquist diagrams of electrochemical impedance spectra of the nanogapped electrode recorded in PBS (0.01 M, pH 7.4) solution containing 0.1 M KCl and 10 mM $Fe(CN)_6^{3-/4-}$. (1) Bare IDA microelectrode with 2.5 μm gap, (2) 25-nm nanogap electrode, and (3) after 3 mM cysteamine modified nanogapped electrode. In panel *a*: scan rate is 100 mV s^{-1}. In panel *b*: the frequency range is from 0.1 Hz to 100 kHz with signal amplitude of 5 mV; the inset is the R_{et} changes in each procedure.

series of self-assembly process is completed when the self-assembled monolayer (SAM) formed by the streptavidin molecules-paved on biotin through one of strongest and specific noncovalent affinities known.

The *in situ* growth of Au NPs which has already plated on the electrode chip was performed by immersing the electrode into a freshly prepared growing solution containing 0.01% $HAuCl_4$ and 0.4 mM $NH_2OH{\cdot}HCl$. SEM images were obtained forcomparison of the gap difference and size of corresponding gold particles before and after the *in situ* seeding growth. As seen in Fig. 3a, before *in situ* seeding growth, Au NPs with size of about 16 ± 1.3 nm were uniformly deposited in the interval between IDA microelectrode arrays after a silanization treatment. However, the gap between neighboring Au NPs (i.e., 61 ± 7.5 nm) is greatly larger than the length of a streptavidin molecule (~4.5 × 4.5 × 5.8 nm^3) [31] used in the present experiment, indicating that the biotin-streptavidin binding cannot efficiently hinder the electron transfer. And the effective sphere of the gold nanoparticles which plays a role in the detection is relatively non-obvious, as will be discussed in equivalent circuit part. One can imagine that there are still a lots of spaces between the neighboring gold nanoparticles. The diameter of Au NPs between IDA microelectrode remains no obvious change (23 ± 1.7 nm) after growth for 30 s, and the gap is relatively tremendous (50 ± 4.9 nm, Fig. 3b). During the next 1 min growth, the size of Au NPs between IDA microelectrode increases to about 33 ± 1.8 nm, but the gap between neighboring AuNPs is still about 42 ± 3.1 nm (Fig. 3c). Upon increasing the growth time further, the diameter of Au NPs increases to 46 ± 2.9 nm and the corresponding nanogaps narrowed to about 25 ± 2.3 nm which can properly accommodate streptavidin (Fig. 3d) by considering the size of biomolecules (The length of self-assembly monolayer of cysteamine, biotin, and streptavidin is about 1–2 nm, 3 nm, and 6 nm) and the stereo-hindrance effect during the specific binding. Fig. 3e and f shows that, with the growth time is increased to 2, 3 min, the diameter of Au NPs is continued growth from 46 ± 2.9 nm to 54 ± 4.9, 63 ± 2.7 nm, respectively, resulting in that the neighboring Au NPs connected together to constitute the electron tunneling path between IDA microelectrodes (Gap size: 20 ± 1.8 nm; 8 ± 1.7 nm). On the basis of the above results, we infer that the 25-nm gold nanogapped electrode was fabricated to detect the streptavidin will possesses high sensitivity. The correlation between length of nanogap and corresponding particle size is summarized in Fig. 3g. Fig. 3h is a UV absorption spectrum of the Au NPs, which reveals that the gold nanoparticle diameter before *in situ* seeding growth is about 16 nm.

The bare IDA microelectrode with 2.5-μm gap, 25-nm nanogap, and cysteamine modified nanogapped electrode were characterized using cyclic voltammogram, complemented with electrochemical impedance spectroscopy (EIS). Fig. 4a presents the cyclic voltammetric responses in a 5 mM $K_3[Fe(CN)_6]$ and 0.1 M KCl mixture solution. In contrast to bare IDA microelectrode, a significant increased peak current is observed at 25-nm gold nanogap electrode. This might be explained by considering the small gap size. That is, when introducing gold nanoparticles into the microgaps, the relative distances between the two adjacent electrodes obviously decreases, facilitating the electron transfer during the redox reaction of $Fe(CN)_6^{3-/4-}$, and the electrochemical probe can also easily approach the working electrode, resulting in an increased current. After decorating cysteamine in the nanogaps, the molecular self-assembly film becomes thick because of the longer molecular chain (ε_i), which could create a barrier for the electrochemical diffusion barrier/electron transfer process. However, owing to the relative low ε_i, the change of peak current is not so much at this stage. From this experiment, we concluded that cysteamine layer had been self-assembled onto the gold nanogapped electrode and obstructed the electron transfer of $Fe(CN)_6^{3-/4-}$ to the electrode surface.

Further confirmation about the layer-by-layer assembly is found by EIS which has been widely used for characterization of modified layers on electrode surfaces. It provides clearer information on the impedance changes of the electrode interface and the semicircle diameter at the higher frequencies equals to the electron transfer resistance (R_{et}), which controls the electron transfer kinetics of the redox probes. R_{et} values of the bare IDA microelectrode, 25-nm nanogap, and cysteamine modified nanogapped electrode were 1061, 106.3, and 150.6 kΩ, respectively, as shown in Fig. 4b.

A device with a 2.5 μm IDAME, a 25-nm nanogap, and a compacted Au NPs nanogap electrode referring to the stage after *in situ* growth for 3 min was studied to confirm that the solution containing biomolecules flows into and fills the nanogapusing cyclic voltammogram and electrochemical impedance spectra (EIS) measurements. All electrodes were dealed with the same assembled procedures under the same experimental conditions. Cyclic voltammograms and Nyquist diagrams of electrochemical impedance spectra are presented in Fig. 5. After biotin-streptavidin binding, the changes of the cyclic voltammograms and EIS showed almost the same tendency for all devices. Fig. 5a and b shows the electrochemical characteristics of the 2.5 μm IDAME before and after biotin-streptavidin binding. The decreased currents in cyclic volatmmogram and the increased resistance in EIS are observed. However, all the electron transfer resistances (R_{et}) are in the range of 1200–1500 kΩ and the increased magnitude is

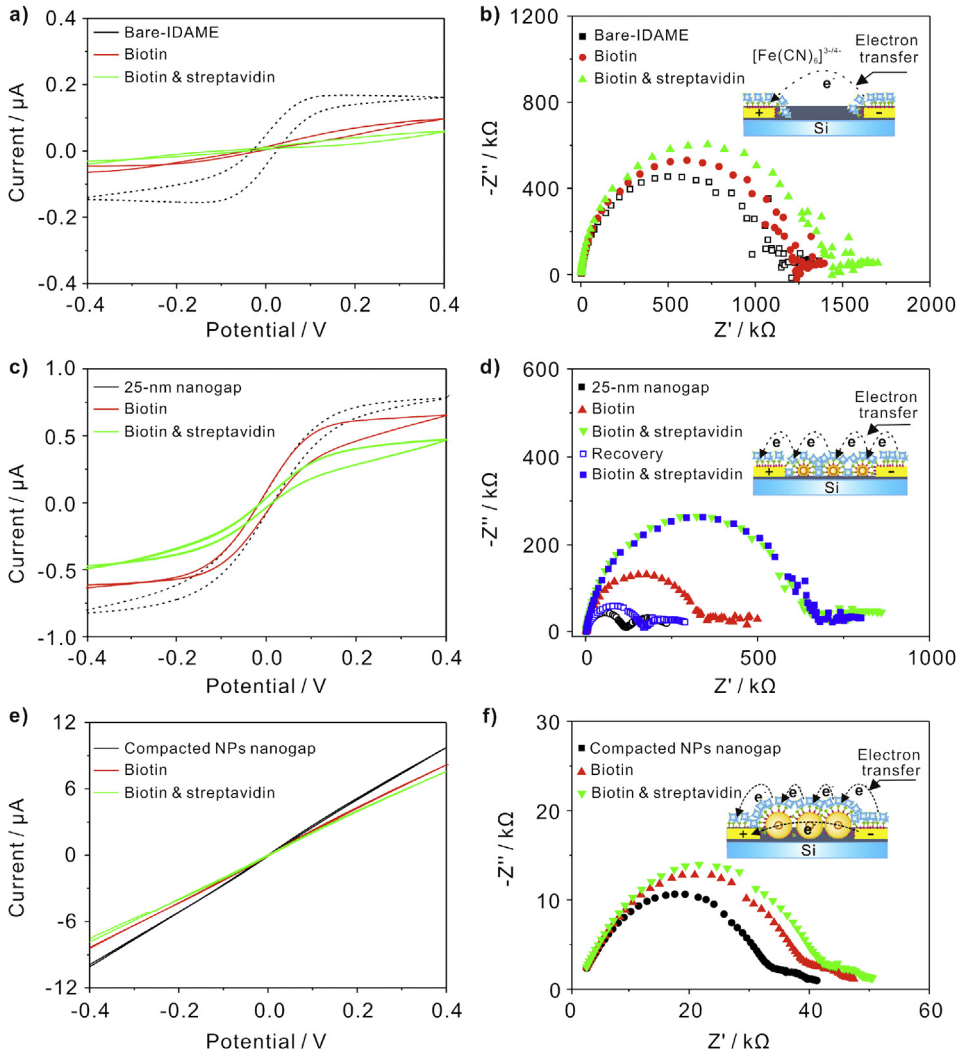

Fig. 5. Cyclic voltammograms and electrochemical impedance spectra of bare IDA microelectrode, 25-nm nanogap, and compacted Au NPs nanogap before and after biomolecules are immobilized in the nanogap in PBS (0.01 M, pH 7.4) solution containing 0.1 M KCl and 10 mM $Fe(CN)_6^{3-}/^{4-}$. (a, b) 2.5 μm IDA microelectrode. (c, d) 25-nm nanogap electrode. (e, f) Compacted Au NPs nanogap electrode referring to the stage after *in situ* growth for 3 min. The inset in panels *b*, *d*, and *f* is the illustration showing electron transfer process in the nanogap. 100 μM biotin and 1 nM streptavidin were used in all measurements, respectively.

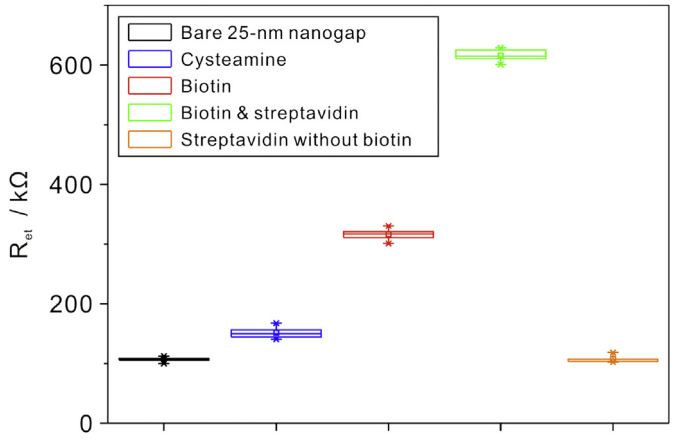

Fig. 6. Statistical results of electron transfer resistance (R_{et}) change of the 25-nm nanogap device in four controlled experiments. The data set for each group was extracted from 20 devices.

negligibly small, indicating that a gap of 2.5 μm length is too wide to create a barrier for inhibiting electron transfer (Inset in Fig. 5b).

In comparison, the changes of both cyclic voltammograms and EIS are sensitive at a 25-nm nanogap electrode after biotin-streptavidin specific binding. As seen in Fig. 5c, the current decreases gradually as biotin and streptavidin was introducing onto the gold nanogap surface. The electron transfer resistance (R_{et}) increases dramatically from 106.3 to 614.7 kΩ after biotin and streptavidin binding (Fig. 5d). In this case, gold nanoparticles can be considered as multiple tiny electrodes, electron transfer between the neighboring gold nanoparticle becomes more smoothly, resulting in a very sensitive detection even though a ultratrace biomolecules were bound (1 nM, Inset in Fig. 5d). Considering that streptavidin molecules are about 6–7 nm in size, most of the 25-nm nanogap is filled when the streptavidin binds to the biotin, and the change in EIS is much larger than in the case of biotin immobilization in bare IDA microelectrode (see Fig. 5b). This indicates that a nanogap of 25-nm length can offer a perfect sized stage for the biomolecular immobilization, and is sufficient to detect biomolecules by means of the EIS change. The biotin-streptavidin binding can be reversibly and efficiently broken with non-ionic

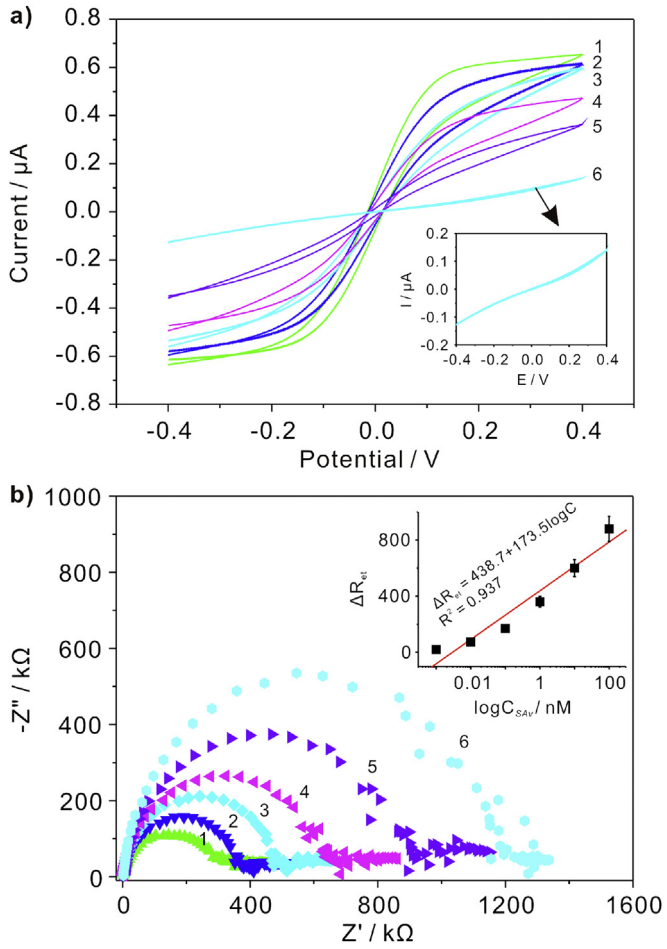

Fig. 7. a) Cyclic voltammograms and b) Nyquist plots of Faradaic impedance spectra of the 25-nm nanogap electrode after biotin-streptavidin binding in PBS (10 mM, pH 7.4) solution containing 0.1 M KCl and 10 mM $Fe(CN)_6^{3-/4-}$. Curves 1–6 represent 0.001, 0.01, 0.1, 1, 10, 100 nM streptavidin addition, respectively. Inset in panel *a* is cyclic voltammogram after 100 nM streptavidin addition; inset in panel *b* is linear relationship between the logarithmic value of the concentration of streptavidin and the electron transfer resistance. EIS was used at scanning frequency range from 0.1 Hz to 100 kHz. Before streptavidin binding, 100 μM biotin was used to modify the nanogap electrode.

aqueous solutions and brief exposure to high temperature (70 °C) [32]. After immersed the device in hot deionized water (70 °C) for 8 min and washed it with deionized water several times, the R_{et} is reversibly shifted to its original state value after breaking the biotin-streptavidin binding (Blue open square, Fig. 5d). Again, we found that the R_{et} goes to the first binding stage after the second-round biotin-streptavidin binding (Blue (in the web version) solid square, Fig. 5d). From this experiment, it is confirmed that the R_{et} shift in the previous experiments can be attributed to the specific biotin-streptavidin binding, and the device provides a satisfactory precision and reproducibility.

As for compacted Au NPs nanogapped electrode, the current significantly reached about 10 μA before biotin-streptavidin binding (black curve, Fig. 5e). And the steady-state current in the sigmodal voltammograms of the microelectrode completely disappeared; the positive scan and negative scan coincides with each other. The impedance decreased obviously from the above several hundred to the dozens of kilohms (Fig. 5f). As having been indicated in Fig. 3g, the statistical analysis shows that the length of a gap is less than 10 nm. In this case, the nanogap can be broken down very easily when applied a certain potential between working and counter electrode; and make the whole circuit possess the electric behavior of semiconductor. On the other hand, the biomolecules cannot fill the gap due to the narrow space, resulting in a slightly change in the current and the impedance (e.g., the impedance merely increased from 33 kΩ to 43 kΩ). Such a little change of electrochemical signal after biotin-streptavidin binding cannot provide an efficient detection. Therefore, it is difficult to use compacted Au NPs nanogapped electrode for biological monitoring.

To check that the stability (Or the electron transfer change results from the functionalization in each step) of the 25-nm nanogap device, we analyzed the statistical results of R_{et} changes in 20 nanogap devices (Fig. 6) with five different groups: bare nanogap, cysteamine, only biotin, biotin-streptavidin, and streptavidin without biotin. We found that the functionalization in each step exhibits a regular and stable R_{et} change and only the biotin-streptavidin group shows the large R_{et} change. Expectedly, R_{et} remains no change for streptavidin without biotin group. From the changes in R_{et} values, therefore, we suggest that biotin-streptavidin binding is the critical factor for changing the electrical characteristics of the 25-nm nanogap device. Thus, it is concluded that the 25-nm nanogap device shows high specificity for detecting biotin-streptavidin binding.

To character the biosensing performance, the 25-nm nanogapped electrode was exposed to various concentrations of streptavidin in buffer. The corresponding cyclic voltammograms and Nyquist plots of electrochemical impedance spectra are shown in Fig. 7. It was found that CV curves reduce gradually with the streptavidin concentration increased (Fig. 7a), attributed to the charge transfer was blocked effectively between electrode surface and the redox probe. The diameter of the Nyquist circle increased with the adding of streptavidin (Fig. 7b). This is likely because more streptavidin molecules bind to the immobilized biotins in higher concentrations of streptavidin, which acts as a definite kinetic barrier for the electron transfer. The nanogap device displayed well-defined concentration dependence. As seen from the inset in Fig. 7b, a linear relation between the relative electron transfer resistance (ΔR_{et}) responses and the logarithmic value of streptavidin concentrations was obtained in a range from 1 pM to 100 nM. The linear regression equation is ΔR_{et} (kΩ) = 438.7(±39.8) + 173.5(±22.4)logC_{SAv} (nM) with a correlation coefficient 0.93 (n = 3). Where ΔR_{et} is calculated by the this equation: $\Delta R_{et} = R_{et(SAv)} - R_{et(Bt)}$, $R_{et(SAv)}$ represents the value of the electron transfer resistance with different concentrations of SAv (streptavidin) specific binding to biotin. $R_{et(Bt)}$ is the value of the biotinylated nanogap electrode impedance before streptavidin binding. When we treated the electron transfer resistance of the streptavidin modified nano-gapped microelectrode as the threshold of the signal, the lowest detectable concentration actually measured is 1 pM. After thoroughly searching literature, it is surprised to find that such a value by electrochemical impedance is even about 5 orders of magnitude higher than that by other FET (field-effect transistor)-based biosensors [32,33]. This specific nano-gapped electrode can be employed to detect streptavidin concentration quantitatively according to the linear equation. This demonstrates that the 25-nm nanogap device sensitively responds to changes in the streptavidin level, producing a linear response over the range of investigated concentrations (ca. 1 pM–100 nM).

4. Conclusion

In summary, we have demonstrated a tunable gold nanogap device coupled with a 25-nm gap that detects the binding of streptavidin to biotin using *electrochemical impedance* technique, without the need for a labeling process. The relative dielectric constant between neighboring Au NPs in the gap area after

streptavidin binding is the dominant factor in detecting the increase in the *electrochemical impedance* spectra. A linear relationship between the change in electron-transfer resistance (ΔR_{et}) and the logarithmic value of streptavidin concentration was established in a range of SAv concentrations from 1 pM to 100 nM. The lowest detection limit of the biosensor actually measured was 1 pM, which is even about 5 orders of magnitude higher than that of several previously reported FET nanogap biosensors. Furthermore, different from most of *electrical* nanogap devices for biosensing, such a nanogap device based on *electrochemical impedance* technique could use to probe the behavior of small amount of molecules in the solution phase which is useful for biological reactions. This result suggested that the combination of *electrochemical impedance* technique and nanogap devices is practically effective in detecting streptavidin. We thus envision a wide range of applications in *lab on a chip* for nucleic acids, protein, antibody-antigen, tumor cells, and pathogenic bacteria analysis where *electrochemical impedance* detection may ultimately prove preferable to the currently more established *electrical* detection techniques.

Acknowledgments

This work was supported by the National Key Scientific Program-Nanoscience and Nanotechnology (2011CB933700), the National natural Science Foundation of China (21105073), and the Project of Educational Committee of Anhui Province (KJ2010B240). Y.W. thanks State Key Laboratory of Electroanalytical Chemistry (SKLEAC201307) and University outstanding youth talent support program of Anhui Province (2014 of Wei), and X.J.H. acknowledges the CAS Institute of Physical Science, University of Science and Technology of China (2012FXCX008), for financial support.

Appendix A. Supplementary data

Supplementary data related to this article can be found at http://dx.doi.org/10.1016/j.aca.2015.11.036.

References

[1] X. Chen, Z. Guo, G.M. Yang, J. Li, M.Q. Li, J.H. Liu, X.J. Huang, Electrical nanogap devices for biosensing, Mater. Today 13 (2010) 28–41.
[2] Y. Fan, X.T. Chen, A.D. Trigg, C.H. Tung, J.M. Kong, Z.Q. Gao, Detection of microRNAs using target-guided formation of conducting polymer nanowires in nanogaps, J. Am. Chem. Soc. 129 (2007) 5437–5443.
[3] J.M. Kong, A.R. Ferhan, X.T. Chen, L. Zhang, N. Balasubramanian, Polysaccharide templated silver nanowire for ultrasensitive electrical detection of nucleic acids, Anal. Chem. 80 (2008) 7213–7217.
[4] C. Fang, Y. Fan, J.M. Kong, Z.Q. Gao, N. Balasubramanian, Electrical detection of oligonucleotide using an aggregate of gold nanoparticles as a conductive tag, Anal. Chem. 80 (2008) 9387–9394.
[5] S. Roy, X.J. Chen, M.H. Li, Y.F. Peng, F. Anariba, Z.Q. Gao, Mass-produced nanogap sensor arrays for ultrasensitive detection of DNA, J. Am. Chem. Soc. 131 (2009) 12211–12217.
[6] X.J. Chen, S. Roy, Y.F. Peng, Z.Q. Gao, Electrical sensor array for polymerase chain reaction-free messenger RNA expression profiling, Anal. Chem. 82 (2010) 5958–5964.
[7] W. Shen, H.M. Deng, Y.Q. Ren, Z.Q. Gao, An electronic sensor array for label-free detection of single-nucleotide polymorphisms, Biosens. Bioelectron. 43 (2013) 165–172.
[8] S. Tokonami, H. Shiigi, T. Nagaoka, Preparation of nanogapped gold nanoparticle array for DNA detection, Electroanalysis 20 (2008) 355–360.
[9] H. Shiigi, Y. Yamamoto, H. Yakabe, S. Tokonami, T. Nagaoka, Electrical property and water repellency of a networked monolayer film prepared from Au nanoparticles, Chem. Commun. (2003) 1038–1039.
[10] S. Tokonami, M. Iwamoto, K. Hashiba, H. Shiigi, T. Nagaoka, Fabrication of a highly sensitive sensor electrode using a nano-gapped gold particle film, Solid State Ionics 177 (2006) 2317–2320.
[11] S. Tokonami, H. Shiigi, T. Nagaoka, Characterization and DNA sensing properties of nanogapped array electrodes, J. Electrochem. Soc. 155 (2008) J105–J109.
[12] S. Tokonami, H. Shiigi, T. Nagaoka, Open Bridge-Structured Gold Nanoparticle Array for Label-Free DNA Detection, Anal. Chem. 80 (2008) 8071–8075.
[13] H. Shiigi, S. Tokonami, H. Yakabe, T. Nagaoka, Label-free electronic detection of DNA-hybridization on nanogapped gold particle film, J. Am. Chem. Soc. 127 (2005) 3280–3281.
[14] J. Zhang, H.G. Nie, Z. Wu, Z. Yang, L.J. Zhang, X.J. Xu, S.M. Huang, Self-catalytic growth of unmodified gold nanoparticles as conductive bridges mediated gap-electrical signal transduction for DNA hybridization detection, Anal. Chem. 86 (2014) 1178–1185.
[15] Y. Yu, X. Chen, Y. Wei, J.H. Liu, S.H. Yu, X.J. Huang, CdSe quantum dots enhance electrical and electrochemical signals of nanogap devices for bioanalysis, Small 8 (2012) 3274–3281.
[16] Y. Yu, X. Chen, Y. Wei, J.H. Liu, X.J. Huang, Strategy for polychlorinated biphenyl detection based on specific inhibition of charge transport using a nanogapped gold particle film, Anal. Chem. 84 (2012) 9818–9824.
[17] Z. Guo, Z.G. Liu, X.Z. Yao, K.S. Zhang, X. Chen, J.H. Liu, X.J. Huang, A molecular-gap device for specific determination of mercury ions, Sci. Rep. 3 (2013).
[18] C. Batchelor-McAuley, E.J.F. Dickinson, N.V. Rees, K.E. Toghill, R.G. Compton, New electrochemical methods, Anal. Chem. 84 (2012) 669–684.
[19] K. Mathwig, S.G. Lemay, Mass transport in electrochemical nanogap sensors, Electrochim. Acta 112 (2013) 943–949.
[20] T. Li, W.P. Hu, Electrochemistry in nanoscopic volumes, Nanoscale 3 (2011) 166–176.
[21] S. Kim, G. Yu, T. Kim, K. Shin, J. Yoon, Rapid bacterial detection with an interdigitated array electrode by electrochemical impedance spectroscopy, Electrochim. Acta 82 (2012) 126–131.
[22] J. Ahn, T.H. Lee, T. Li, K. Heo, S. Hong, J. Ko, Y. Kim, Y.B. Shin, M.G. Kim, Electrical immunosensor based on a submicron-gap interdigitated electrode and gold enhancement, Biosens. Bioelectro 26 (2011) 4690–4696.
[23] X.J. Chen, Y.Y. Wang, J.J. Zhou, W. Yan, X.H. Li, J.J. Zhu, Electrochemical impedance immunosensor based on three-dimensionally ordered macroporous gold film, Anal. Chem. 80 (2008) 2133–2140.
[24] X.J. Chen, K. Zhang, J.J. Zhou, J. Xuan, W. Yan, L.P. Jiang, J.J. Zhu, Electrochemical immunosensor based on colloidal carbon sphere array, Biosens. Bioelectro 25 (2010) 1130–1136.
[25] C.M. Ruan, L.J. Yang, Y.B. Li, Immunobiosensor chips for detection of Escherichia coli O157 : H7 using electrochemical impedance spectroscopy, Anal. Chem. 74 (2002) 4814–4820.
[26] M.A. Panagopoulou, D.V. Stergiou, I.G. Roussis, M.I. Prodromidis, Impedimetric biosensor for the assessment of the clotting activity of rennet, Anal. Chem. 82 (2010) 8629–8636.
[27] L.J. Yang, Y.B. Li, G.F. Erf, Interdigitated array microelectrode-based electrochemical impedance immunosensor for detection of Escherichia coli O157 : H7, Anal. Chem. 76 (2004) 1107–1113.
[28] G. Pelossof, R. Tel-Vered, S. Shimron, I. Willner, Controlling interfacial electron transfer and electrocatalysis by pH- or ion-switchable DNA monolayer-modified electrodes, Chem. Sci. 4 (2013) 1137–1144.
[29] J. Turkevich, P.C. Stevenson, J. Hillier, A study of the nucleation and growth processes in the synthesis of colloidal gold, Dicuss. Faraday Soc. 11 (1951) 55–75.
[30] G. Frens, Controlled nucleation for the regulation of the particle size in monodisperse gold suspensions, Nat. Phys. Sci. 241 (1973) 20–22.
[31] K.K. Caswell, J.N. Wilson, U.H.F. Bunz, C.J. Murphy, Preferential end-to-end assembly of gold nanorods by biotin-streptavidin connectors, J. Am. Chem. Soc. 125 (2003) 13914–13915.
[32] H.S. Im, X.J. Huang, B. Gu, Y.K. Choi, A dielectric-modulated field-effect transistor for biosensing, Nat. Nanotechnol. 2 (2007) 430–434.
[33] D.S. Kim, J.E. Park, J.K. Shin, P.K. Kim, G. Lim, S. Shoji, An extended gate FET-based biosensor integrated with a Si microfluidic channel for detection of protein complexes, Sens. Actuat. B Chem. 117 (2006) 488–494.